Journal of Power Sources 306 (2016) 541–551

Contents lists available at ScienceDirect

Journal of Power Sources

journal homepage: www.elsevier.com/locate/jpowsour

Effect of the incorporation of sulfonated chitosan/sulfonated graphene oxide on the proton conductivity of chitosan membranes

Abbas Shirdast, Alireza Sharif*, Mahdi Abdollahi

Department of Polymer Reactions Engineering, Faculty of Chemical Engineering, Tarbiat Modares University, P.O. Box: 14155/143, Tehran, Iran

HIGHLIGHTS

- Sulfonated chitosan (SCS) and SGO are added to CS to prepare nanocomposite membranes.
- Nanocomposite membranes show better thermal/mechanical properties than pure CS.
- SCS and SGO enhance proton conductivity of CS in a synergistic manner.
- Adding 5 wt% SGO to CS/SCS causes about 6-fold gain in conductivity and selectivity.
- Experimental proton conductivity data are predicted by a Nernst–Planck based model.

GRAPHICAL ABSTRACT

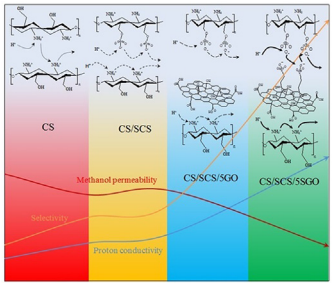

ARTICLE INFO

Article history:
Received 30 August 2015
Received in revised form
15 December 2015
Accepted 16 December 2015
Available online xxx

Keywords:
Chitosan
Fuel cell
Proton conductivity
Graphene oxide
Sulfonation
Modeling

ABSTRACT

Chitosan biopolymer (CS) has been attracting considerable interest as polymer electrolyte in fuel cells. However, proton conductivity of chitosan is low and it is necessary to enhance its conductivity. In this work, 10 wt% sulfonated chitosan (SCS) and different amounts of sulfonated graphene oxide (SGO) nanosheets are incorporated into a chitosan membrane to investigate their effects on the electrochemical properties of the membrane. The proton conductivity and methanol permeability tests conducted on the CS/SCS/SGO membranes show that the conductivity is increased by 454%, the permeability is reduced by 23% and hence the selectivity is increased by 650%, relative to the neat chitosan, at SGO content of 5 wt%. Furthermore, combined addition of SCS and SGO to chitosan causes much more proton conductivity enhancement than the individual additives due to the synergistic effect of SCS and SGO. The observed synergistic effect reveals the importance of the chemical functionality of chitosan and nanofillers in the formation of ionic cluster domains with enhanced size within the membranes for proton transport. Finally, a Nernst–Planck based model is applied to the experimental proton conductivity data in order to shed more light on the role of GOs in the proton conductivity mechanism of chitosan.

1. Introduction

In the past decade, direct methanol fuel cells (DMFCs) have gained considerable attention as power sources for portable power applications owing to many advantages such as high energy density, no requirement of fuel reforming process, simplicity and

* Corresponding author.
E-mail address: asharif@modares.ac.ir (A. Sharif).

http://dx.doi.org/10.1016/j.jpowsour.2015.12.076
0378-7753/

convenience [1–3].

Proton exchange membrane (PEM) is one of the major components which directly govern the DMFC performance. Perfluorosulfonic acid (PFSA) membranes (e.g. Nafion) are currently the most widely used fuel cell membranes for DMFCs, due to their high proton conductivity and good chemical stability [4]. However, these membranes suffer from high methanol permeability, which diminishes the fuel cell efficiency and performance [5]. Moreover, the high cost of Nafion has impeded the commercialization of DMFC technology so far. In recent years, chitosan (CS), an abundant and inexpensive polysaccharide with low toxicity, has been suggested as a promising membrane material for DMFC applications, mainly due to its inherent low methanol permeability [6]. Nevertheless, chitosan membranes show low proton conductivity, and therefore, there is an urgent need to enhance their conductivity. There are two main approaches to improve proton conductivity. The first is the functionalization of chitosan with different groups, especially sulfonic acid, $-SO_3H$, groups. For example, Xiang et al. [7] prepared a sulfonated chitosan (SCS) polymer by grafting the chitosan monomers with sulfonic groups in order to be used as PEM [7]. Due to the excessive swelling of the SCS, it was blended with pure chitosan in different weight ratios and cross-linking was occurred by the bonds reaction between the sulfonic groups in SCS and the amide groups in the pure chitosan monomers. It was found that the developed CS/SCS membranes had enhanced proton conduction and methanol resistance compared to pure CS membrane. Nevertheless, the proton conductivity enhancement and methanol permeability reduction were not sufficient enough to result in a high selectivity (the ratio of proton conductivity and methanol permeability) compared to Nafion. Addition of inorganic fillers has been another approach to improve the proton conductivity of chitosan membranes [8–10]. Embedding inorganic fillers within the membrane also plays important roles in enhancing mechanical and thermal properties and suppressing methanol crossover. A variety of fillers, including montmorillonite, silica, titania, metal oxides, metal phosphates and zeolites have been incorporated in chitosan membranes for fuel cell applications [11–15].

Recently, Bai et al. [15] fabricated chitosan nanohybrid membranes containing halloysite nanotubes bearing sulfonate polyelectrolyte brushes (SHNTs) for potential DMFC PEMs. It was shown that the high aspect nanotube and long polyelectrolyte brush allow SHNTs to construct continuous and wide pathways along which sulfonic acid–amide acid–base pairs are formed and work as low-barrier proton-hoping sites, imparting an enhanced proton transfer via Grotthuss mechanism.

Compared with HNTs, functionalized graphene oxide (F-GO) nanosheets allow protons to permeate through them with selectively rejecting other substances, such as methanol, due to the ability to form unique two-dimensional nanochannels between the sheets [16]. Thus, fabricating and investigating F-GO containing chitosan membranes would facilitate the development of promising PEMs with high selectivity for DMFC applications.

In this work, we prepared nanocomposites consisting of a chitosan/sulfonated chitosan blend (CS/SCS) as the matrix and sulfonated graphene oxide (SGO) nanosheets as the filler to study the effects of both SCS and SGO on the proton conductivity and selectivity of the chitosan. The results demonstrated the synergistic effect of SCS and SGO on the proton conductivity enhancement of CS. In addition, the facilely functionalized GO nanosheets were found to be highly efficient in improving the selectivity of chitosan.

On the other hand, compared with a huge amount of experimental studies regarding the effects of micro/nano particles on the proton conductivity of polymeric membranes, studies devoted to predict the proton conductivity are scarce in the literature [17,18]. Consequently, another objective of this work was to apply a recently developed Nernst–Planck based model [17] to our experimental proton conductivity data in order to describe the role of GOs in the proton conductivity mechanism of chitosan as well as to extend the applicability of the model to a broader category of PEMs.

2. Theory

A Nernst–Planck based model has been proposed by Choi et al. [19] to predict the proton conductivity (σ_H^+) of neat and spherical nanoparticle-containing polymeric electrolytes:

$$\sigma_{H^+} = \frac{\varepsilon_i}{\tau}\left[\frac{F^2}{RT}\left(D_H^{\Sigma} + C_H^{\Sigma} + D_H^{G} + C_H + D_H^{E} + C_{H^+}\right)\right] \tag{1}$$

where F is the Faraday constant (96485C mol^{-1}), R is the molar gas constant (8.314 J $mol^{-1}K^{-1}$), T is temperature (K) and $D_{H^+}^{\Sigma} D_{H^+}^{G}$ and $D_{H^+}^{E}$ are diffusion coefficients of protons for the surface, Grotthuss and en masse diffusion mechanisms, respectively. Also, $C_{H^+}^{\Sigma}$ represents concentration of protons participating in surface diffusion while C_{H^+} is concentration of protons participating in Grotthuss and en masse diffusions. The detailed equations for calculating diffusion coefficients and concentrations of protons can be found in Ref. [17]. Furthermore, ε_i and τ are porosity of the membrane and the tortuosity factor, respectively.

The porosity of nanocomposite membranes can be given as follows [20]:

$$\varepsilon_i = \frac{\lambda_w\left(1/EW_M + w/MW_p\right)}{\lambda_w\left(1/EW_M + w/MW_p\right) + r_{M/W}\Big/EW_M + w.r_{p/w}\Big/MW_p} \tag{2}$$

where w, λ_w, $r_{M/W}$ and $r_{p/w}$ represent the weight percent of nanoparticles, moles of water sorbed per acid site, the ratio of partial molar volume of membrane to that of water and the ratio of partial molar volume of nanoparticles to that of water, respectively. Moreover, EW_M is equivalent weight of the host membrane and MW_p is the molecular weight of nanoparticles, estimated by equivalent weight of the nanoparticles, EW_p.

Recently, our group [17] developed the Choi model to consider the exact role of graphene oxide based nanosheets in the proton conductivity mechanism of polymeric membranes. It was found that the expression employed for calculating the tortuosity factor, as the ratio of the actual distance to the shortest distance that a proton travels through a membrane, of the Choi model played an important role in whether the experimental data was accurately predicted. The following equation was then suggested for calculating the overall tortuosity factor (τ') of GO containing PEM's [17]:

$$\tau' = \frac{\tau\left(1 + \frac{a\varphi}{6}\right)}{(1-\varphi)\left(1 + \frac{a\varphi}{6}\right) + \tau\varphi} \tag{3}$$

where, τ, a and φ are the host membrane tortuosity, aspect ratio of nanoparticles and volume fraction of nanoparticles, respectively. The membrane tortuosity factor (τ) in eq. (3) can be obtained from Prager [21] or Yasuda models [22] (τ_p or $\tau_{Y,k}$, respectively):

$$\tau_p = \frac{2(1-\varepsilon_i) + 2\varepsilon_i \ln \varepsilon_i - 0.5\varepsilon_i(\ln \varepsilon_i)^2}{\varepsilon_i(1-\varepsilon_i) + \varepsilon_i^2 \ln \varepsilon_i} \tag{4}$$

$$\tau_{Y,K} = \exp(K((1/\varepsilon_i) - 1)) \tag{5}$$

In eq. (5), the K parameter is a size coefficient whose value has been reported to be 0.7 or 3 depending on the chemical structure of

the membrane and the relative size of the penetrant molecules [23]. By inserting K = 0.7 or 3 into eq. (5), $\tau_{Y,0.7}$ or $\tau_{Y,3}$ expressions will be obtained, respectively. Finally, employing τ_p, $\tau_{Y,0.7}$ or $\tau_{Y,3}$ expressions in eq. (3) would result in τ'_P, $\tau'_{Y,0.7}$ or $\tau'_{Y,3}$ expressions, respectively, as the overall tortuosity factors.

3. Experimental

3.1. Materials

Chitosan (medium molecular weight, degree of deacetylation: 80%) was supplied from Sigma–Aldrich. Taurine (2-aminoethanesulfonic acid) was purchased from Samchuon. Sulfuric acid (98%), potassium permanganate (99.9%), graphite powder (>99.5%), hydrogen chloride (37%), hydrogen peroxide (35%), chlorosulfonic acid (98%), diethyl ether, sodium bicarbonate ($NaHCO_3$), acetic acid and sodium hydroxide were obtained from Merck.

3.2. Sulfonation of graphene oxide

Graphene oxide nanoparticles (GO) were synthesized using natural graphite powder according to the modified hummer's method [24,25]. Introduction of sulfonic acid groups on GO was carried out by a nucleophilic reaction between epoxy groups of graphene oxide and amine groups of taurine as shown in Scheme 1.

The reaction was carried out in water at a temperature of 60 °C under nitrogen atmosphere for 72 h, with 0.002:0.137:0.859 weight ratios of GO, taurine and water, respectively. The prepared samples were filtered and washed with water to remove the precursor residue. Finally, the product (SGO) was dried at room temperature for 24 h.

3.3. Synthesis of sulfonated chitosan

Sulfonated chitosan (SCS) was synthesized according to the method reported previously [7]. Scheme 2 depicts the synthesis route schematically. A homogeneous solution of chlorosulfonic acid (20 ml) and sulfuric acid (40 ml) was prepared and cooled down to 4 °C. Then 1 g of chitosan was added to the solution and dissolved by stirring for 60 min at room temperature. The final product was precipitated by 200 ml of cold diethyl ether and filtered. The aqueous solution of the obtained SCS was neutralized to pH 7 with 0.5 M $NaHCO_3$, dialyzed against DI water for 2 days, and then isolated by lyophilization.

3.4. Preparation of the membranes

The membranes were fabricated by the solution-casting method. The CS or CS/SCS membranes were prepared by first dissolving the chitosan or chitosan/sulfonated chitosan (10/1, wt/wt), respectively, in an aqueous acetic acid (2 wt%) solution. Then, the solutions were cast on glass plates and left in ambient air for 7 days, and then dried at 60 °C for 2 h. In order to prepare nanocomposite membranes with CS/SCS as the matrix, and SGO as the filler, various quantities of SGO (0.5, 5 or10 wt%) were dispersed in water. Also, appropriate amounts of CS/SCS (10/1, wt/wt) were completely dissolved in an aqueous acetic acid (2 wt%) solution. Subsequently, the nanosheet suspensions were mixed with the CS/SCS solutions and stirred for 5 h at room temperature to obtain homogeneous dispersions containing different amounts of the SGO nanosheets. Afterward, the solutions were cast on glass Petri dishes and kept at room temperature for 7 days, and then dried at 60 °C for 2 h in order to complete the solvent evaporation process. It should be noted that CS nanocomposite membranes containing 5 wt% GO or SGO nanosheets and CS/SCS nanocomposite membrane containing 5 wt% GO nanosheets were also prepared via the above procedure to elucidate the exact role of SGO and SCS on the properties and characteristic of chitosan. Table 1 shows the designation and composition of the prepared membranes.

All the dry membranes were immersed in NaOH solution (2 mol L-1) for 30 min to remove the residual acetic acid and then thoroughly washed with water until a neutral pH was obtained. The membranes (CS membrane, CS/SCS membrane and nanocomposite ones) were also immersed in 0.5 M sulfuric acid solution for 24 h to completely crosslink the CS matrix and then washed with DI water to remove the residual acid and dried under vacuum at 25 °C for 24 h.

3.5. Characterization of nanoparticles and membranes

Fourier Transform Infrared, FTIR, spectra of the nanoparticles and membranes were recorded with a Perkin–Elmer spectrophotometer, USA, in the range of 4000–400 cm^{-1}. Atomic Force Microscopy (AFM, CP-Research, ThermoMicroscopes/Veeco, USA) was utilized to characterize the thickness of graphene oxide (GO) and sulfonated graphene oxide (SGO). The samples for AFM were prepared by dropping aqueous GO or SGO solution ($\approx$0.05 mg mL^{-1}) onto a fresh mica wafer, followed by drying it at room temperature for 24 h. The AFM image was recorded in a tapping mode under ambient conditions. X-ray diffraction (XRD) patterns of the nanosheets and membranes were obtained using an X-ray diffractometer (X'Pert MPD model, Philips, Holland) equipped with Cu Kα. The tube was operated at 40 kV, 30 mA.

Thermogravimetry (TG) and differential scanning calorimetry (DSC) analyses of the membranes were measured using a DSC-TGA analyzer (V5.1A Dupont 2000, USA). The temperature measurement ranged from room temperature up to 400 °C at a scan rate of 20 °C min^{-1} under nitrogen atmosphere. Mechanical properties of the samples were determined on the GOTECH test instrument (GT-

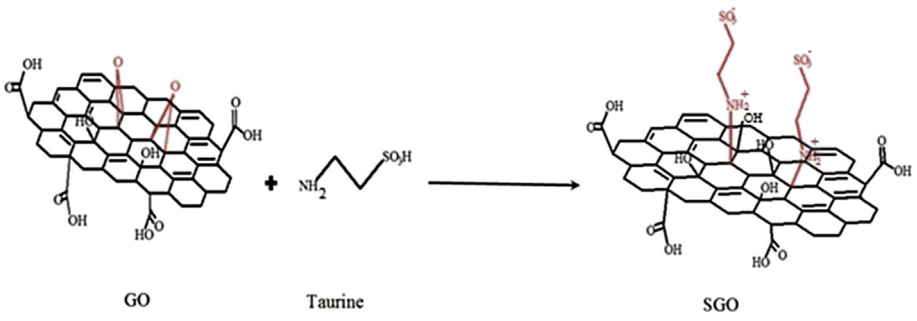

Scheme 1. Sulfonation of graphene oxide.

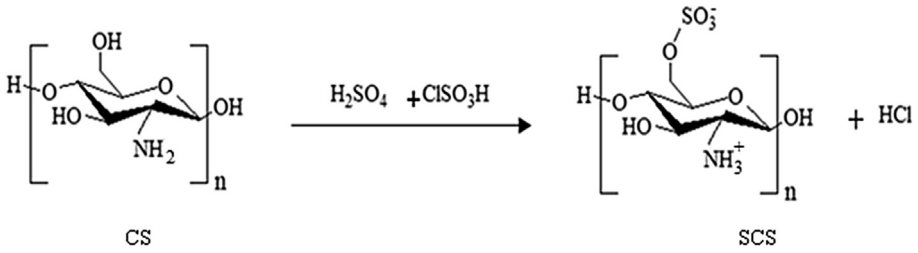

Scheme 2. Synthesis of sulfonated chitosan.

Table 1
Designation and composition of the membranes.

Membrane	CS/SCS (wt/wt)	GO (wt%)	SGO (wt%)
CS	10/0	–	–
CS/SCS	10/1	–	–
CS/5SGO	10/0	–	5
CS/5GO	10/0	5	
CS/SCS/0.5SGO	10/1	–	0.5
CS/SCS/5SGO	10/1	–	5
CS/SCS/10SGO	10/1	–	10
CS/SCS/5GO	10/1	5	–

TCS-2000, Taiwan), according to ASTM D638, at a crosshead speed of 3 mm min^{-1}.

3.6. Water uptake and swelling ratio

The CS based membranes were dried in vacuum at 60 °C for 24 h, and their weights and volumes were measured (W_{dry} and V_{dry}, respectively). The membranes were then immersed in deionized water at 25 °C for 24 h. The surfaces of the wetted membranes were dried with tissue paper and their new weights and volumes were measured (W_{wet} and V_{wet}, respectively). The water uptake (WU) and swelling ratio (SW) were calculated from eqs (6) and (7), respectively:

$$WU\% = \left(W_{wet} - W_{dry}\right) \Big/ W_{dry} \times 100 \quad (6)$$

$$SW\% = \left(V_{wet} - V_{dry}\right) \Big/ V_{dry} \times 100 \quad (7)$$

3.7. Ion exchange capacity (IEC) and proton conductivity

The Ion exchange capacity (IEC) of the membranes was determined by a titration method. Dry membranes were weighted (W_{dry}) and immersed in 100 ml of a NaCl solution (1 M) for 24 h to replace the H^+ with Na^+.

The quantity of H^+ released from the membranes was determined by titration, using a 0.01 M NaOH solution with phenolphthalein as the indicator. Finally, the IEC value (meq g^{-1}) was obtained by the following equation:

$$IEC = \left(V_{NaOH} \times N_{NaOH}\right) \Big/ W_{dry} \quad (8)$$

where, V_{NaOH} and N_{NaOH} are the consumed volume and molarity of the NaOH solution.

Proton conductivity of the membranes was measured by a two-probe method using an Autolab PGSTAT303N potentiostat/galvanostat Impedance Analyzer (Ecochemie). The spectra were recorded with signal amplitude of 5 mV in the frequency range of 0.1 Hz-10^5 Hz. The samples were fully hydrated in water for 48 h prior to test at room temperature. The proton conductivity (σ, S cm^{-1}) was calculated by the following equation:

$$\sigma = L/AR \quad (9)$$

where L, A and R indicate the membrane thickness, membrane area and membrane resistance(Ω), respectively. R was obtained from the high-frequency intercept of the impedance.

3.8. Methanol permeability & selectivity

Methanol permeability of the prepared membranes was measured using a glass diffusion cell. The cell consists of two compartments of 100 mL capacity, divided by a membrane sample. One chamber of the cell (V_A) was filled with an aqueous methanol solution (2 M) and the other chamber (V_B) was filled with DI water. After equilibration with deionized water for 12 h, the membrane sample (1 × 1 cm^2) was clamped between the two chambers.

Methanol permeated across the membrane due to a concentration gradient between the two chambers. The methanol flux was analyzed using gas chromatography equipped with FID detector (Philips PU 4410). Methanol permeability (P, $cm^2 s^{-1}$) was then determined via:

$$P = \frac{1}{C_A}\left(\frac{\cdot C_B}{\cdot t}\right)\left(\frac{L\,V_B}{A}\right) \quad (10)$$

where C_A, $\left(\frac{\cdot C_B}{\cdot t}\right)$, V_B, L and A indicate methanol concentration in compartment A (mol L^{-1}), slope of change in methanol concentration in compartment B (mol L^{-1} s^{-1}), volume of compartment B (mL), thickness of the membrane (cm) and effective membrane area (cm^2), respectively. Finally, selectivity (SP, S scm^{-3}) was estimated as:

$$SP = \sigma/P \quad (11)$$

4. Results and discussion

4.1. Characterization of the nanoparticles

Fig. S1 (Supplementary information) shows the FTIR spectra of GO and SGO nanoparticles. The FTIR spectrum of GO shows C=O stretching absorption band at 1729 cm^{-1}. The bands due to the C–O in alcohol or epoxy groups (COH/COC) appear in the range of 1450–1000 cm^{-1}. In addition, the peak at 1440 cm^{-1} is attributed to the O–H bending vibration of alcohol or COOH units and the resonance at 1620 cm^{-1} to the adsorbed water or skeletal ring vibrations of un-oxidized graphitic domains [26,27].

The successful grafting of taurine on the surface of graphene oxide is confirmed by comparing the FTIR spectra of GO and SGO. In

the SGO sample the peaks associated with C–N and SO_3H groups of taurine appear at about 1049 and 1220 cm^{-1}, respectively. Also, the peak at 1620 cm^{-1} is ascribed to the amide N–H group of the sulfonating agent.

Fig. S2 represents XRD patterns of the nanoparticles. The shifting of the parent graphite peak ($2\theta = 26.6°$, d-spacing = 3.33 Å) to a lower angle ($2\theta = 12.4°$, d-spacing = 0.82 nm) for GO sheets indicates the complete transformation from graphite stacks to graphene oxide nanosheets. Further increase of d-spacing of the SGO sheets to 0.86 nm ($2\theta = 10.69°$) is believed to be due to the existence of sulfonic acid groups on their surfaces.

Typical AFM images and the corresponding height profiles of the nanoparticles are shown in Fig. S3. The AFM height profile of GO particles denotes the full exfoliation of parent graphite powder into individual, single-layer graphene oxide sheets [28,29]. On the other hand, due to the presence of sulfonic acid groups on SGO surfaces, the sheets are slightly thicker (around 1.76 nm) than GOs.

4.2. Characterization of the membranes

Chitosan and chitosan/sulfonated chitosan blend can be well mixed with graphene oxide and sulfonated graphene oxide to form homogeneous and stable aqueous solutions at room temperature [30,31]. Actually, the many amino and hydroxyl groups and also the polycationic nature of chitosan in acid media cause electrostatic attraction and hydrogen bonding between CS or CS/SCS and GO or SGO, inducing the truly homogeneous dispersion of the components on the molecular scale [32]. For example, the FTIR analysis of CS/SCS and CS/SCS/5SGO membranes are conducted to confirm the hydrogen bonding interaction between SGO and the matrix, Fig. 1.

The spectrum of CS/SCS membrane shows characteristic absorbance bands of C=O stretching vibration of amide I and amide II groups at 1646 cm^{-1} and 1544 cm^{-1}, respectively. Furthermore, the appeared peak at 820 cm^{-1} corresponds to the specific absorbance of C–O–S groups of the SCS chains [7]. The peaks of amide I and amide II groups of CS/SCS are shifted from 1646 cm^{-1} and 1544 cm^{-1} to 1635 cm^{-1} and 1535 cm^{-1}, respectively, in the spectrum of CS/SCS/5SGO membrane, Fig. 1. Moreover, the O–H group band of CS/SCS is shifted from 3431 cm^{-1} to 3260 cm^{-1}, by introducing SGO nanosheets to the membrane. These results clearly indicate the formation of hydrogen bond between CS/SCS and SGO [33,32].

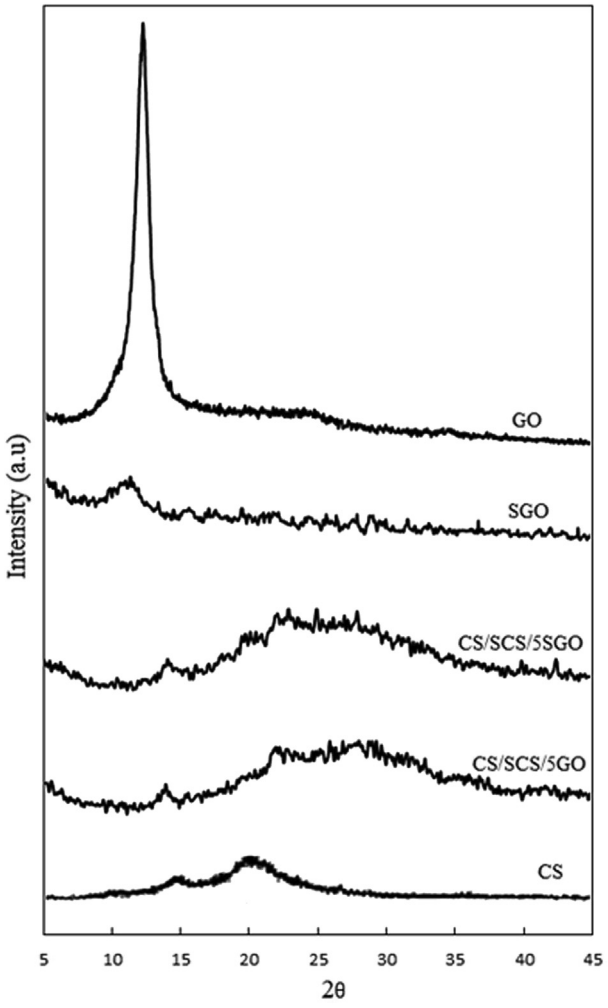

Fig. 2. XRD patterns of CS, CS/SCS/5GO, CS/SCS/5SGO, GO and SGO.

To determine the quality of the nanofillers dispersion in

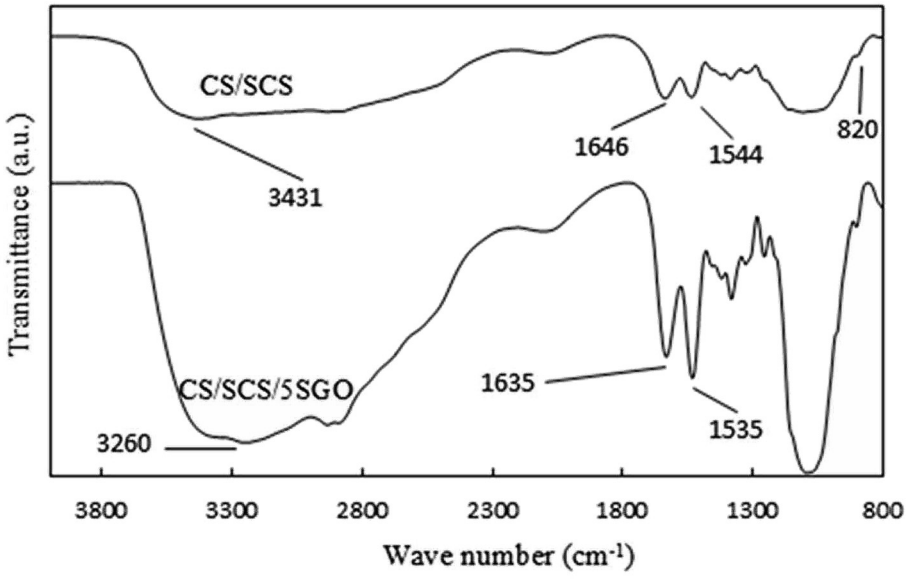

Fig. 1. FTIR spectra of CS/SCS and CS/SCS/5SGO membranes.

chitosan based matrices, X-ray diffraction (XRD) was employed. Fig. 2 shows the XRD patterns of the (CS/SCS)/5GO and (CS/SCS)/5SGO membranes along with those of the pure chitosan membrane, GO and SGO samples. There is a peak at about 15° in the pattern of all the membranes, corresponding to the crystalline structure of the chitosan. Furthermore, the peak appeared at 21°, in the pattern of the pure chitosan membrane, as well as those appeared at around 27°, in the patterns of the nanocomposite membranes, are related to the amorphous structure of the chitosan. Interestingly, due to the nanosheet induced crystallization of the nanocomposites, the intensity of the characteristic peaks of nanocomposite membranes at 15° is slightly higher than that of the CS. In other words, the electrostatic interaction and hydrogen bonding between CS/SCS and GO or SGO can contribute to an ordered arrangement of the attached polymer chains along the rigid GO or SGO sheets [32].

As can be seen from Fig. 2, diffraction peaks of GO and SGO completely disappear from the XRD patterns of the nanoparticle containing membranes, indicating the formation of fully exfoliated structure of GO and SGO sheets in the matrices and the disappearance of the regular and periodic structure of graphene oxide.

4.3. Thermal and mechanical properties of the membranes

Thermal stability of polymer electrolyte membranes strongly affects the performance of fuel cells. Investigation of thermal properties of the membranes was performed by TGA and DSC analysis. Fig. 3 shows TGA curves of CS/SCS, CS/SCS/0.5SGO and CS/SCS/5SGO membranes, demonstrating a three-stage weight loss for the membranes: the first stage involves evaporation of physically adsorbed water molecules from the membranes (20–190 °C); the second stage involves degradation of chitosan side-chains (190–250 °C) and the third stage is related to degradation of polymer backbone (over 285 °C) [11]. It is seen that the weight loss over 190 °C is decreased by increasing the SGO content of the membranes. This result implies higher thermal stability of the nanocomposite membranes, in comparison to CS/SCS membrane. The thermal stability enhancement can be ascribed to favorable interfacial interactions, such as hydrogen-bonding or electrostatic interactions between the CS/SCS matrix and sulfonated graphene oxide nanosheets [7,15].

Further investigation of thermal properties by DSC measurements, Fig. 4, shows endothermic peaks at $T_d = 230$, 232 and 234 °C in the thermograms of CS/SCS, CS/SCS/0.5SGO and CS/SCS/5SGO, respectively, corresponding to the second weight-loss stage of TGA results, Fig. 3. The endothermic area (A_e) increases from 63.274 J g^{-1} for CS/SCS to 81.38 J g^{-1} for CS/SCS/5SGO. In agreement with the FTIR, XRD and TGA results, the increases of T_d and A_e values by increasing the SGO content, points to an effective attachment of polymer chains to the SGO sheets and the resultant constraining of the segmental motion of the chains by hydrogen bonding and electrostatic attraction.

Moreover, adequate mechanical stability is necessary for PEMs during membrane-electrode assembly fabrication. Table 2 represents the modulus and tensile strength of the membranes. Addition of sulfonated chitosan increases the modulus and tensile strength of the chitosan membrane by 36% and 35%, respectively. These enhancements can be due to the formation of cross-linking network in the blend membrane [7]. Also, incorporation of GO and SGO nanosheets into the chitosan or blend membranes, enhances the modulus and tensile strength of the corresponding nanocomposite membranes. As shown in Table 2 addition of 5 wt% GO or SGO increases the modulus of pure CS by 40% or 50%, respectively, and increases the tensile strength by 45% or 78%, respectively. Moreover, the corresponding increases in the tensile properties of CS/SCS blend as a result of the incorporation of 5 wt% GO or SGO are 37% or 38%, respectively, for modulus and 35% or 45%, respectively, for tensile strength. By comparing the tensile behavior of nanocomposite membranes, one can find that SGO nanoparticles are more effective in improving the mechanical properties of CS or CS/SCS samples than GOs, indicating important role of the interactions between the nanoparticles and matrix in this improvement. Furthermore, the modulus and tensile strength of the nanocomposite membranes increase gradually with the increasing loading of SGO. The dependence of the modulus and tensile strength on the content of sulfonated graphene oxide is probably ascribed to molecular-level dispersion of SGOs and the strong H-bonding between the CS/SCS and the surface of sulfonated graphene oxide [30]. Overall, the prepared membranes are strong and flexible enough for fuel cell applications.

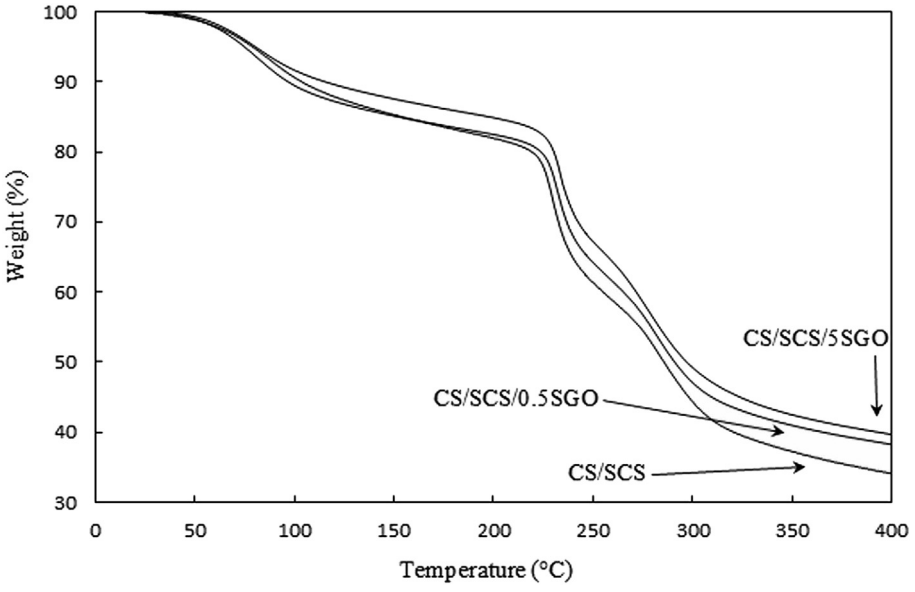

Fig. 3. TGA curves of CS/SCS, CS/SCS/0.5SGO and CS/SCS/5SGO.

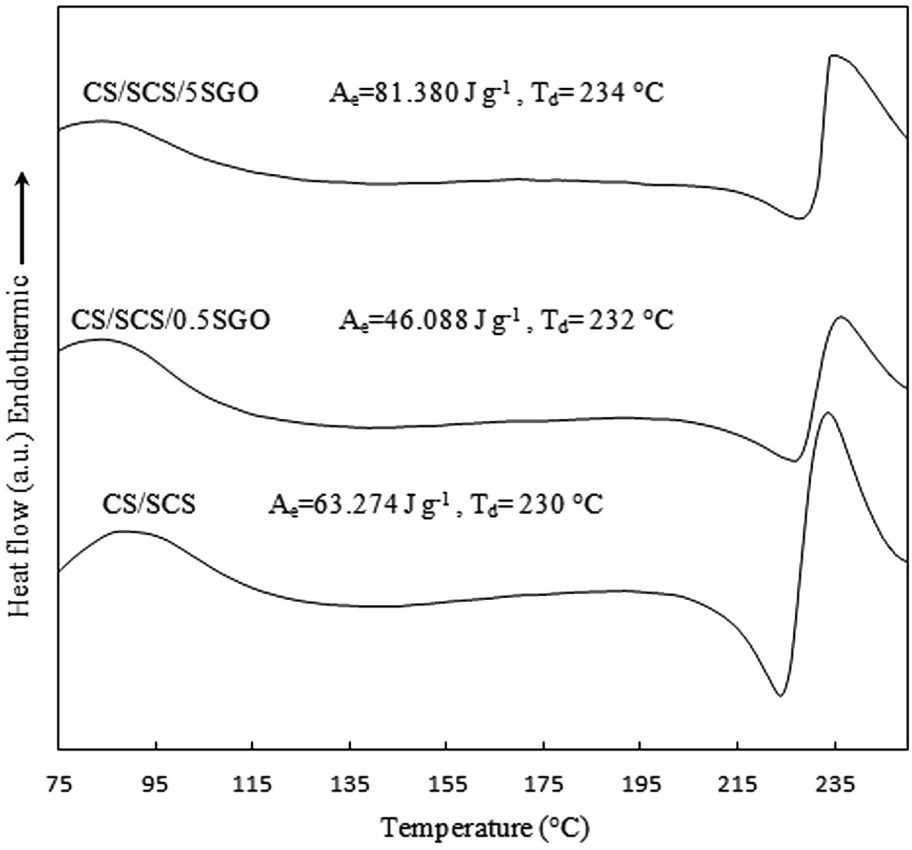

Fig. 4. DSC curves of CS/SCS, CS/SCS/0.5SGO and CS/SCS/5SGO.

Table 2
Mechanical properties, water uptake and swelling ratio of the pure chitosan, blending and nanocomposite membranes.

Membrane	Modulus (MPa)	Tensile strength (MPa)	WU%	SW%
CS	167.5 ± 11.7	72.4 ± 3.6	55.5 ± 2.7	47 ± 2
CS/SCS	227.0 ± 15.9	96.9 ± 4.8	31.2 ± 1.5	41 ± 2
CS/5GO	232.8 ± 16.3	105.0 ± 5.2	82.0 ± 4.1	55 ± 2
CS/5SGO	255.3 ± 17.8	129.5 ± 6.4	75.5 ± 3.7	48 ± 2
CS/SCS/5GO	312.0 ± 21.8	131.0 ± 6.5	76.2 ± 3.8	49 ± 2
CS/SCS/0.5SGO	251.5 ± 17.5	125.3 ± 6.2	58.2 ± 2.9	47 ± 2
CS/SCS/5SGO	315.0 ± 22.0	140.0 ± 7.0	65.2 ± 3.2	48 ± 2
CS/SCS/10SGO	377.0 ± 26.4	155.8 ± 7.8	61.0 ± 3.0	50 ± 2

4.4. Water uptake & swelling ratio of the membranes

High water uptake would be beneficial for proton conduction via both vehicle and Grotthuss mechanisms in a PEM, provided that it does not cause swelling problems in the membrane. The water uptake (WU) and swelling ratio (SW) of all the membranes are shown in Table 2. As can be seen addition of both GO and SGO nanoparticles increases the WUs of the CS and CS/SCS membranes. This phenomenon is attributed to the hygroscopic nature of graphene oxide [34] and the presence of functional groups on the surfaces of introduced fillers (hydroxyl groups on GO and sulfonic acid groups on SGO) which helps in absorbing more water. Recently, Zarrin et al. [35] also reported an increase in WU of Nafion, as a result of functionalized graphene oxide loading. In comparison, the 5wt% GO containing membranes show higher water uptake values than the 5 wt% SGO containing membranes. This can be due to the weaker GO-CS or GO-CS/SCS interfacial interactions, relative to SGO-CS or SGO-CS/SCS interfacial interactions, and the resultant more free volume in the GO containing membranes. Furthermore, it can be inferred from Table 2 that the incorporation of GO-based nanosheets into CS-based polymer matrices leads to the formation of hydrogen bonding and electrostatic forces between the nanosheets and polymers, thus increasing the water-absorbing capacity without sacrificing the mechanical properties. For example, adding 10 wt% SGO simultaneously leads to ~30% increase in WU and ~60% increase in tensile strength (Table 2) of the CS/SCS membrane.

4.5. IEC, proton conductivity and methanol permeability

IEC plays a significant role in proton conductivity of DMFCs, since it provides a direct measure of the number of milli-equivalents of ions in 1 g of the prepared membranes. Table 3 shows IEC values of the membranes. CS/SCS shows a higher IEC value (0.97 meq g^{-1}) than the pure chitosan membrane (0.65 meq g^{-1}), due to the existence of sulfonic acid groups in the structure of sulfonated chitosan. With incorporating GO nanosheets in the CS or CS/SCS membranes, the IEC values of the membranes are slightly decreased. The decrease is ascribed to the dilution effect of adding GOs, which lack sulfonic acid groups and thus reduce the concentration of available protons in GO containing membranes. On the other hand, because of the increasing of concentration of sulfonic acid groups originated from incorporated SGO nanosheets, IECs of SGO containing membranes are higher than those of the corresponding nanoparticle-free membranes. Investigation of IEC values of CS/SCS as a function of SGO loading (Table 3) demonstrates that 10 wt% SGO containing membrane possesses lower IEC than 5 wt% SGO containing one, in spite of the higher concentration of ionic groups in the former system. The

Table 3
IEC, hydrated thickness, proton conductivity, methanol permeability and selectivity of the pure chitosan, blending and nanocomposite membranes.

Membrane	IEC (meq g^{-1})	Thickness (μm)	Proton conductivity (σ, mS cm^{-1})	Methanol permeability (P, × 10^{-8} cm^2 s^{-1})	Selectivity (SP × 10^4 S s cm^{-3})
CS	0.65 ± 0.03	71 ± 1	1.30 ± 0.06	6.20 ± 0.31	2.09 ± 0.14[a]
CS/SCS	0.97 ± 0.05	71 ± 1	2.20 ± 0.11	5.91 ± 0.29	3.72 ± 0.26
CS/5GO	0.60 ± 0.03	72 ± 1	1.90 ± 0.09	6.31 ± 0.31	3.01 ± 0.21
CS/5SGO	0.85 ± 0.05	71 ± 1	3.30 ± 0.16	6.12 ± 0.30	5.39 ± 0.37
CS/SCS/5GO	0.94 ± 0.05	73 ± 1	2.80 ± 0.14	6.03 ± 0.30	4.64 ± 0.33
CS/SCS/0.5SGO	0.98 ± 0.05	74 ± 2	4.80 ± 0.24	5.50 ± 0.27	8.72 ± 0.61
CS/SCS/5SGO	1.20 ± 0.06	74 ± 2	7.20 ± 0.36	4.75 ± 0.24	15.15 ± 0.99
CS/SCS/10SGO	1.04 ± 0.06	76 ± 2	6.10 ± 0.30	4.62 ± 0.23	13.20 ± 0.92

[a] The estimated error for the selectivity values due to uncertainties in determination of proton conductivity and methanol permeability values.

reason may be the tendency of the SGO sheets to restacking with increasing SGO content in the membrane to more than 5 wt%, thereby some of the sulfonic acid groups between nanosheets are inactivated [33].

According to the results of proton conductivity (σ) measurements, Table 3, the CS membrane shows a proton conductivity value of 0.0013 S cm^{-1}, lower than those usually reported for chitosan in the literature [15,36]. This is due to lower degree of deacetylation of chitosan of the present work (80%), in comparison with those utilized by other researchers (over 90%) [15,7]. By incorporating 10 wt% sulfonated chitosan, the CS proton conductivity is increased to 0.0022 S cm^{-1}. It should be noted that CS/SCS has lower water uptake and thus less proton carriers than CS, Table 2. However, sulfonic acid groups introduced by SCS increase the IEC and proton hopping sites of the CS/SCS, Table 3. Therefore, Grotthuss mechanism is believed to be responsible for the enhanced proton conductivity of CS/SCS membrane, relative to CS one. Also, the proton conductivities of CS and CS/SCS are slightly increased as a result of adding 5 wt% GO nanosheets, Table 3. Regarding the fact that GO nanosheets lack sulfonic acid groups, one can conclude that the higher water uptake of GO containing membranes, Table 2, leads to the enhancement of their proton conductivities compared to those of the filler-free membranes, via vehicle mechanism. On the other hand, incorporating only 0.5 wt% SGO nanosheets causes an almost 2-fold improvement in the proton conductivity of CS/SCS membrane. Moreover, the proton conductivities of CS/SCS/5SGO (0.0072 Scm^{-1}) and CS/SCS/10SGO (0.0061 Scm^{-1}) are 3.3 and 2.8 time, respectively, higher than that of the CS/SCS. In these cases, ion clusters of hydrophilic sulfonic acid groups, introduced by SGO nanosheets and SCS, form well-connected channels in the membranes through which protons can be transported quickly. Consequently, since SGO nanosheets, also increase water uptake capacity of the membranes, Table 2, we believe that such improvements in the proton conductivity of CS/SCS membrane are due to both Grotthuss and vehicle mechanisms, strengthened by the SGO particles. However, it is seen that there is an optimum loading amount of SGO (about 5 wt%) which leads to a maximum proton conductivity in the CS/SCS system. As Table 3 demonstrates, adding 10 wt% SGO presumably increases the tortuous path for proton transport and inhibited the movement of CS/SCS chains in the ionic clusters which eventually results in a proton conductivity value lower than that of the CS/SCS/5SGO.

The Nyquist and Bode-modulus plots for CS/SCS and CS/SCS/5SGO membranes are shown in Fig. 5, under fully hydrated condition at 25 °C. The nanocomposite membrane displays a lower resistance (higher proton conductivity) than that of the blend membrane, Fig. 5(a). Also, Bode-modulus plots (Fig. 5) (b) shows lower resistance for CS/SCS/5SGO membrane, confirming the result obtained from the Nyquist plots.

Further inspection of the data presented in Table 3 reveals the synergistic effect of sulfonated chitosan and sulfonated graphene oxide on proton conductivity of chitosan. In other words, the effect of the co-existence of SCS and SGO on conductivity enhancement of pure chitosan is greater than the algebraic sum of their separate effects, as presented in Table 4. In contrast, no synergistic effect is observed in proton conductivity of chitosan with a combination of SCS and GO nanosheets, Table 4. The observed synergistic effect indicates the importance of the chemical functionality of nanofillers and chitosan in the counterbalance between the electrostatic energy released by ion–dipole interactions ($SO_3^-H^+$) and the elastic free energy due to the deformation of backbone chains, leading to the formation of ionic cluster domains with enhanced size within the membranes for proton transport [16].

Another requirement for successful application of a polymeric membrane in DMFC is its low methanol permeability (P). Table 3 also shows methanol permeability of the prepared membranes. The CS sample shows a methanol permeability value of 6.20 × 10^{-8} cm^2s^{-1}, which is near 2 orders of magnitude lower than that of Nafion 117 (2.91 × 10^{-6} cm^2s^{-1}) [33]. Blending the CS with sulfonated chitosan decreases its methanol permeability to 5.91 × 10^{-8} cm^2s^{-1}. However, when GO is added to the CS or CS/SCS matrix, methanol permeability is slightly increased. The weak adhesion between polymer matrix and nanosheets gives rise to cavities, which favor molecular diffusion. In contrast, by the addition of functionalized GOs, the membrane's void volume is reduced because of strong H-bonding, leading to slower diffusion of the penetrants and lower methanol permeability. As can be seen from Table 3, incorporating 0.5, 5 and 10 wt% SGO into the CS/SCS membrane reduces the methanol permeability by 7, 20 and 22%, respectively.

The overall membrane performance as a PEM is usually evaluated in terms of selectivity parameter (SP = σ/P). A higher SP value means better applicability in DMFCs. Table 3 demonstrates that SGO nanosheets significantly increase SP values of chitosan based membranes. For instance, CS/SCS/5SGO membrane exhibits about 7-fold greater SP value than that for CS membrane. Furthermore, in comparison with the Nafion 117 membrane (SP = 3.5 × 10^4 S s cm^{-3} [35]), the 5 wt% SGO containing CS/SCS membrane shows an almost 4-fold enhancement in the SP value. This may be attributed to improved proton conductivity and reduced methanol permeability of CS/SCS/SGO nanocomposite membranes, in comparison with pristine CS/SCS membrane.

Proton conductivity and selectivity of the current state-of-the-art membranes have been reported in the literature to be in the ranges of 0.05–0.1 S cm^{-1} and 3 × 10^4 – 9 × 10^4 S s cm^{-3}, respectively. However, proton conductivity and selectivity of the CS/SCS/5SGO membrane, showing the best performance among the membranes prepared in the present work, were 0.0072 S cm^{-1} and 15 × 10^4 S s cm^{-3}, respectively. The lower conductivity of the above chitosan based nanocomposite membrane can be accounted for by the low proton conductivity of the base chitosan membrane (0.0013 S cm^{-1}, Table 3). If optimal amounts of SCS and SGO are

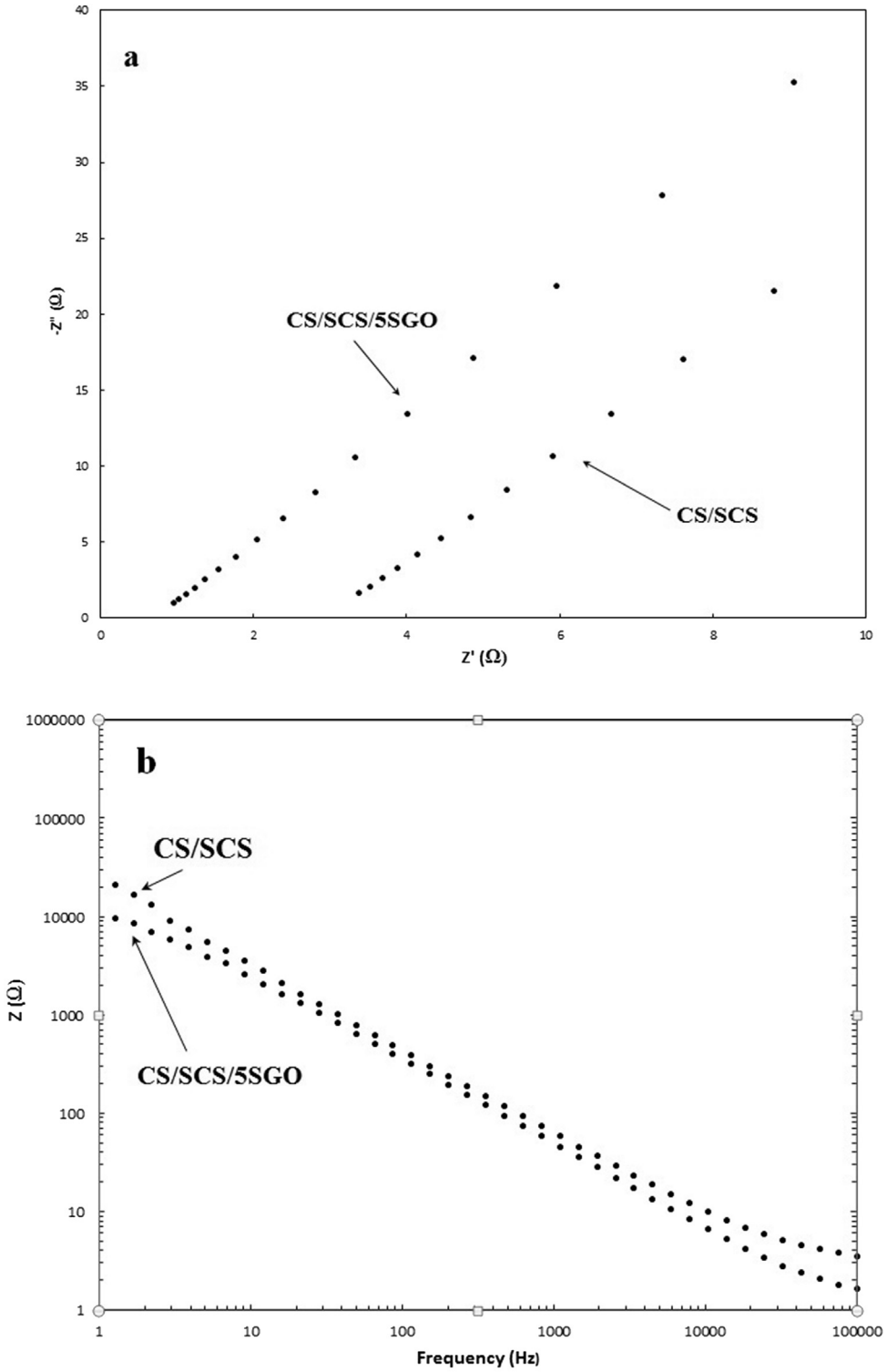

Fig. 5. Nyquist (a) and Bode-modulus (b) plots for CS/SCS and CS/SCS/5SGO membranes.

Table 4
The effect of adding SCS, GO and SGO on the proton conductivity enhancement of pure chitosan membrane and demonstration of synergistic effect in combined addition of SCS and SGO.

Proton conductivity enhancement of pure chitosan						
SCS	GO (5wt%)	SGO (5wt%)	SCS + 5 wt% GO (Algebraic sum)	SCS + 5 wt% GO (Experimental)	SCS + 5 wt% SGO (Algebraic sum)	SCS + 5 wt% SGO (Experimental)
69%	46%	154%	115%	115%	223%	454%

used within a chitosan membrane possessing higher initial conductivity, the conductivity of the resultant nanocomposite membrane is expected to synergistically increase and approach those of the high performance membranes. On the other hand, the low methanol permeability and considerably high selectivity values reported in the present work, for chitosan membranes, would suggest the promising potentials and long-term stability of SGO-containing chitosan-based membranes in DMFC applications.

4.6. Prediction of proton conductivity

Table 5represents the required parameters for calculating proton conductivity of the membranes by eq (1). Also, Table 6 shows the moles of water loading per acid sites (λ_w) for all membranes, obtained by the following equation [20].

$$\lambda_w = WU/(MW_w \cdot IEC) \quad (12)$$

where, WU is the water uptake (WU%/100), IEC is the ion exchange capacity and MW_w is water's molecular weight.

Table 7 demonstrates the relative error (RE) between the experimental and predicted proton conductivity values for each membrane. Note that the table includes RE values obtained by using the tortuosity factors taken from the Prager equation (τ_p), Yasuda equations ($\tau_{Y,0.7}$ and $\tau_{Y,3}$) and their modified forms (τ'_P, $\tau'_{Y,0.7}$ and $\tau'_{Y,3}$, respectively) in eq (1). We recently showed that in order to predict proton conductivity of non-fluorinated membrane systems by eq (1), the selection of the best expression for tortuosity factor calculations depends on the IEC values of the host membranes [17]. It was concluded that in non-fluorinated membranes, possessing low IEC values (<1 meq g^{-1}) the results obtained by substituting the Yasuda equation in eq. (1) are more consistent with experimental data. In agreement with this finding, we observe that the use of modified Yasuda equation (K = 3), $\tau'_{Y,3}$, to estimate the tortuosity factor in eq (1) gives the best agreement (the least RE values) between experimental and calculated proton conductivity values of the chitosan based nanocomposite membranes (Table 7).

Table 6
Moles of water loading per acid sites for the membranes.

Membrane	λ_w
CS	47.4
CS/SCS	17.8
CS/5GO	75.9
CS/5SGO	49.3
CS/SCS/5GO	45.0
CS/SCS/0.5SGO	32.9
CS/SCS/5SGO	30.2
CS/SCS/10SGO	32.5

Table 7
Relative error[a] between the experimental and predicted proton conductivity values for each membrane.

Membrane	τ_p	τ'_p	$\tau_{Y,3}$	$\tau'_{Y,3}$	$\tau_{Y,0.7}$	$\tau'_{Y,0.7}$
CS	23	23	8	8	32	32
CS/SCS	15	15	5	5	30	30
CS/5GO	20	26	10	5	28	33
CS/5SGO	22	28	9	6	26	31
CS/SCS/5GO	17	18	10	7	30	32
CS/SCS/0.5SGO	20	22	6	4	29	35
CS/SCS/5SGO	25	28	7	5	31	34
CS/SCS/10SGO	21	23	6	3	29	33

[a] $RE(\%) = \frac{\sigma_{exoerimental} - \sigma_{predicted}}{\sigma_{exp\ erimental}} \times 100$

Table 5
Parameters required for calculating proton conductivity of the membranes.

Parameter	Value	Unit	Comment
GO properties			
t	1	nm	Thickness of GO sheets
$\rho_{f\text{-}GO}$	2.2	$g\ cm^{-3}$	Density of GO[11]
$IEC_{f\text{-}GO}$	0	$meq\ g^{-1}$	Ion exchange capacity of GO
a	952.38		Aspect ratio of GO
$l_{\sum,GO}$	0	nm	Jump length of surface proton for acid groups of GO [17]
SGO properties			
t	1.7	nm	Thickness of SGO sheets
$\rho_{f\text{-}GO}$	2.2	$g\ cm^{-3}$	Density of SGO [11]
$IEC_{f\text{-}GO}$	4.5	$meq\ g^{-1}$	Ion exchange capacity of SGO
$MW_{f\text{-}GO}$	222.22	$g\ mol^{-1}$	Molecular weight of SGO
$R_{f(f\text{-}GO)}$	0.254	nm	Radius of acid site of SGO [20]
a	625		Aspect ratio of SGO
$\varepsilon_{r(f\text{-}GO)}$	6		Relative permittivity of SGO [20]
$r_{p/w}$	5.55		Molar volume ratio of SGO to Water
$l_{\sum,SGO}$	0.255	nm	Jump length of surface proton for acid sites of SGO [17]
CS membrane properties			
P_{CS}	0.73	$g\ cm^{-3}$	Density of chitosan host membrane
IEC_{CS}	0.65	$meq\ g^{-1}$	Ion exchange capacity of chitosan membrane
EW_{CS}	1538.46	$g\ mol^{-1}$	Equivalent weight of chitosan host membrane
$r_{CS/W}$	117.08		Molar volume ratio of chitosan host membrane to water
$\varepsilon_{r(CS)}$	6		Relative permittivity of CS [20]
$l_{\sum,CS}$	0.255	nm	Jump length of surface proton for amine sites of CS [17]
$R_{f(CS)}$	0.254	nm	Radius of amine sites of CS [20]
CS/SCS membrane properties			
$P_{CS/SCS}$	0.73	$g\ cm^{-3}$	Density of chitosan/sulfonated chitosan membrane
$IEC_{CS/SCS}$	0.97	$meq\ g^{-1}$	Ion exchange capacity of chitosan/sulfonated chitosan membrane
$EW_{CS/SCS}$	1030.92	$g\ mol^{-1}$	Equivalent weight of chitosan/sulfonated chitosan membrane
$r_{(CS/SCS)/W}$	78.45		Molar volume ratio of chitosan/sulfonated chitosan membrane to water
$l_{\sum,CS/SCS}$	0.255	nm	Jump length of surface proton for amine and acid sites of CS/SCS [17]
$R_{f(cs/scs)}$	0.254	nm	Radius of acid and amine sites of CS/SCS [20]
$\varepsilon_{r(CS/SCS)}$	6		Relative permittivity of CS/SCS [20]

This is primarily attributed to the poor continuity of proton transport channels within the low-IEC CS and CS/SCS membranes whose effect is reasonably taken into account by the Yasuda equation [17]. Also, due to the small size of the proton transport channels within these low-IEC membranes, the Yasuda equation with lower size parameter (K = 0.7), corresponding to larger channels [23], does not agree with the experimental data, as satisfactorily as the Yasuda equation with higher size parameter (K = 3) does. Furthermore, the fact that the use of $\tau'_{Y,3}$ expression instead of $\tau_{Y,3}$ one in eq. (1) results in lower RE values, Table 7, reveals the well dispersion of GO and SGO nanosheets in the host membranes and their significant effects on the final proton conductivities.

5. Conclusions

Chitosan based nanocomposite membranes were prepared by incorporating GO or SGO nanosheets into CS or CS/SCS matrices. Favorable interactions between the nanosheets and matrices were confirmed via FTIR and XRD methods. Moreover, the positive effects of the nanosheets on the thermal and mechanical properties of chitosan based polymers were revealed by using TGA, DSC and mechanical tester. The results of proton conductivity and methanol permeability measurements showed that 5 wt% containing CS/SCS membrane possessed a selectivity value about 7 times greater than that of the neat chitosan. Interestingly, simultaneous addition of SCS and SGO to chitosan enhanced the chitosan proton conductivity in a synergistic manner. However, the synergistic effect was not observed with a combination of SCS and GO nanosheets. The above synergistic effect points to the significance of the chemical functionality of both chitosan and GO in the formation of ionic clusters with optimum domain size for proton transport. We also suggest that the recently developed model based on the Nernst–Planck approach is efficient in predicting the proton conductivity and designing new generations of graphene oxide containing PEMs.

Acknowledgment

Partial financial support from the Iranian Nano-technology Initiative is gratefully appreciated.

Appendix A. Supplementary data

Supplementary data related to this article can be found at http://dx.doi.org/10.1016/j.jpowsour.2015.12.076.

References

[1] G.J.M. Janssen, M.L.J. Overvelde, J. Power Sources 101 (2001) 117–125.
[2] M. Winter, R.J. Brodd, Chem. Rev. 104 (2004) 4245–4270.
[3] R. Shahabadi, M. Abdollahi, A. Sharif, Int. J. Hydrogen Energy 40 (2015) 3749–3761.
[4] H. Wu, B. Zheng, X. Zheng, J. Wang, W. Yuan, Z. Jiang, J. Power Sources 173 (2007) 842–852.
[5] Z.Z. Gu, J. Ding, N. Yuan, F. Chu, B. Lin, Int. J. Hydrogen Energy 38 (2013) 16410–16417.
[6] P. Mukoma, B.R. Jooste, H.C.M. Vosloo, J. Power. Sources 136 (2004) 16–23.
[7] Y. Xiang, M. Yang, Z. Guo, Z. Cui, J. Membr. Sci. 337 (2009) 318–323.
[8] J.R. Salgado, Electrochim. Acta 52 (2007) 3766–3778.
[9] V.T. Magalad, S.S. Pattanashetti, G.S. Gokavi, M.N. Nadagouda, T.M. Aminabhavi, Chem. Eng. J. 189–190 (2012) 1–4.
[10] Y.L. Liu, Y.H. Su, J.Y. Lai, Polymer 45 (2004) 6831–6837.
[11] Y. Wang, D. Yang, X. Zheng, Z. Jiang, J. Li, J. Power. Sources 183 (2008) 454–463.
[12] Y. Yin, T. Xu, X. Shen, H. Wu, Z. Jiang, J. Membr. Sci. 469 (2014) 355–363.
[13] H. Wu, W. Hou, J. Wang, L. Xiao, Z. Jiang, J. Power. Sources 195 (2010) 4104–4113.
[14] J. Wang, Y. Zhao, W. Hou, J. Geng, L. Xiao, H. Wu, Z. Jiang, J. Power. Sources 195 (2010) 1015–1023.
[15] H. Bai, H. Zhang, Y. He, J. Liu, B. Zhang, J. Wang, J. Membr. Sci. 454 (2014) 220–232.
[16] B.G. Choi, J. Hong, Y.C. Park, D.H. Jung, W.H. Hong, P.T. Hammond, H. Park, ACS Nano 5 (2011) 5167–5174.
[17] A. Shirdast, A. Sharif, M. Abdollahi, Int. J. Hydrogen Energy 39 (2014) 1760–1768.
[18] Z. Taherkhani, M. Abdollahi, A. Sharif, J. Electrochem. Soc. 162 (2015) F1096–F1100.
[19] P. Choi, N.H. Jalani, R. Datta, J. Electrochem. Soc. 152 (2005) E123–E130.
[20] P. Choi, N.H. Jalani, R. Datta, J. Electrochem. Soc. 152 (2005) A1548–A1554.
[21] S. Koter, J. Membr. Sci. 206 (2002) 201–215.
[22] H.W. Osterhoudt, J. Phys. Chem. 78 (1974) 408–411.
[23] R.F. Prini, M. Philipp, J. Phys. Chem. 80 (1976) 2041–2046.
[24] Y. Gao, M. Hu, B. Mi, J. Membr. Sci. 455 (2014) 349–356.
[25] H. Koolivand, A. Sharif, M.R. Kashani, M. Karimi, M.K. Salooki, M.A. Semsarzadeh, J. Polym. Res. 21 (2014) 599–610.
[26] Z. Jiang, X. Zhao, A. Manthiram, Int. J. Hydrogen Energy 38 (2013) 5875–5884.
[27] D.C. Lee, H.N. Yang, S.H. Park, W.J. Kim, J. Membr. Sci. 452 (2014) 20–28.
[28] J. Lu, W. Liu, H. Ling, J. Kong, G. Ding, D. Zhou, X. Lu, RSC Adv. 2 (2012) 10537–10543.
[29] Y. Wang, Z. Shi, J. Fang, H. Xu, J. Yin, Carbon 49 (2011) 1199–1207.
[30] D. Han, L. Yan, W. Chen, W. Li, Carbohydr. Polym. 83 (2011) 653–658.
[31] S. Anandhavelu, S. Thambidurai, Electrochim. Acta 90 (2013) 194–202.
[32] X. Yang, Y. Tu, L. Li, S. Shang, X.M. Tao, ACS Appl. Mater. Interfaces 2 (2010) 1707–1713.
[33] Y. Heo, H. Im, J. Kim, J. Membr. Sci. (2013) 425–426, 11–22.
[34] A. Bagri, C. Mattevi, M. Acik, Y.J. Chabal, M. Chhowalla, V.B. Shenoy, Nat. Chem. 2 (2010) 581–587.
[35] H. Zarrin, D. Higgins, Y. Jun, Z. Chen, M. Fowler, J. Phys. Chem. C 115 (2011) 20774–20781.
[36] Z. Cui, W. Xing, C. Liu, J. Liao, H. Zhang, J. Power. Sources 188 (2009) 24–29.